OXFORD

SOT | Society of Toxicology
academic.oup.com/toxsci

TOXICOLOGICAL SCIENCES, 177(1), 2020, 140–155

doi: 10.1093/toxsci/kfaa085
Dryad Digital Repository DOI: http://doi:10.5061/dryad.8931zcrn3
Advance Access Publication Date: 11 June 2020
Research Article

Exposure Effects Beyond the Epithelial Barrier: Transepithelial Induction of Oxidative Stress by Diesel Exhaust Particulates in Lung Fibroblasts in an Organotypic Human Airway Model

Samantha C. Faber,* Nicole A. McNabb,† Pablo Ariel,‡ Emily R. Aungst,† and Shaun D. McCullough †,1

*Curriculum in Toxicology and Environmental Medicine, UNC Chapel Hill, Chapel Hill, North Carolina 27599 †Public Health and Integrated Toxicology Division, Center for Public Health and Environmental Assessment, US Environmental Protection Agency, Chapel Hill, North Carolina 27599 and ‡Microscopy Services Laboratory, Department of Pathology and Laboratory Medicine, University of North Carolina at Chapel Hill, Chapel Hill, North Carolina 27599

Disclaimer: The contents of this article have been reviewed by the U.S. Environmental Protection Agency and approved for publication and do not necessarily represent Agency policy. Mention of trade names or commercial products does not constitute endorsement or recommendations for use.

[1]To whom correspondence should be addressed at Public Health and Integrated Toxicology Division, US Environmental Protection Agency, EPA Human Studies Facility, 104 Mason Farm Road, CB #7315, Chapel Hill, NC 27599. Fax: 919-966-6271. E-mail: mccullough.shaun@epa.gov.

ABSTRACT

In vitro bronchial epithelial monoculture models have been pivotal in defining the adverse effects of inhaled toxicant exposures; however, they are only representative of one cellular compartment and may not accurately reflect the effects of exposures on other cell types. Lung fibroblasts exist immediately beneath the bronchial epithelial barrier and play a central role in lung structure and function, as well as disease development and progression. We tested the hypothesis that *in vitro* exposure of a human bronchial epithelial cell barrier to the model oxidant diesel exhaust particulates caused transepithelial oxidative stress in the underlying lung fibroblasts using a human bronchial epithelial cell and lung fibroblast coculture model. We observed that diesel exhaust particulates caused transepithelial oxidative stress in underlying lung fibroblasts as indicated by intracellular accumulation of the reactive oxygen species hydrogen peroxide, oxidation of the cellular antioxidant glutathione, activation of NRF2, and induction of oxidative stress-responsive genes. Further, targeted antioxidant treatment of lung fibroblasts partially mitigated the oxidative stress response gene expression in adjacent human bronchial epithelial cells during diesel exhaust particulate exposure. This indicates that exposure-induced oxidative stress in the airway extends beyond the bronchial epithelial barrier and that lung fibroblasts are both a target and a mediator of the adverse effects of inhaled chemical exposures despite being separated from the inhaled material by an epithelial barrier. These findings illustrate the value of coculture models and suggest that transepithelial exposure effects should be considered in inhalation toxicology research and testing.

Key words: *in vitro*; coculture; oxidative stress; lung; fibroblast; transepithelial; epithelial.

Exposure to inhaled chemicals is a ubiquitous part of daily life that occurs as a result of environmental chemicals/air pollutants, consumer products, occupational environments, and pharmaceuticals. Protecting public health requires identifying potentially toxic chemicals and materials, as well as their cellular and molecular mechanisms of action. The diverse range of chemicals and complex nature of exposure scenarios precludes directly testing all new and existing inhalable materials and chemicals in relevant doses, time courses, and mixtures using the *in vivo* animal exposure studies that are currently required by regulatory agencies. To overcome this limitation, the National Academy of Sciences (NAS) developed a long-range plan, *Toxicity Testing in the 21st Century: A Vision and a Strategy*, to increase the human relevance of toxicity testing while reducing study cost and duration by increasing the usage of *in vitro* and computational approaches (Collins *et al.*, 2008; Kleinstreuer *et al.*, 2014; National Research Council, 2007). Since the NAS report, inhalation toxicology has relied heavily on *in vitro* systems composed solely of bronchial epithelial cells, which form the barrier layer that separates inhaled materials from underlying lung tissue. Although invaluable to inhalation toxicology to date, these monoculture models (ie, culture model with only one cell type) do not include key components of the cellular microenvironment that exist *in vivo* (eg, interactions with adjacent cell types). Thus, they are unable to assess the role of other cell types in the airway microenvironment as potential targets and/or mediators of inhaled chemical exposure effects. Fibroblasts are an integral component of the airway microenvironment that reside immediately beneath the airway epithelial barrier (Figure 1A) and occupy approximately 75% of the total volume of the interstitial space in the adult lung (Bradley *et al.*, 1980). They also mediate airway structure and function, lung disease, and postinjury lung repair (Kendall and Feghali-Bostwick, 2014; White, 2015). Despite their abundance and importance in the airway, the role of lung fibroblasts in the effects of inhaled chemical exposures is poorly understood. As a result, current approaches may under- or overpredict potential adverse effects of chemical exposures.

The adverse effects of chemical exposures are often associated with their ability to generate oxidative species (eg, reactive oxygen species) that exceed the capacity of cellular antioxidants, resulting in redox imbalance (Deavall *et al.*, 2012). Oxidative stress occurs when redox imbalance leads to the alteration of cellular processes and plays a role in acute and chronic airway inflammation (MacNee, 2001; Poli *et al.*, 2004). Diesel exhaust particulates are a ubiquitous air pollutant and principal constituent of fine (aerodynamic diameter of $\leq$ 2.5 μm) ambient particulate matter that induce pulmonary oxidative stress and cause significant morbidity and mortality from chronic obstructive pulmonary disease (COPD), asthma, pulmonary inflammation, airway hyperresponsiveness, susceptibility to pulmonary infection, ischemic heart disease, and congestive heart failure (United States Environmental Protection Agency, 2019). Despite the diverse nature of diesel exhaust particulate exposure effects, investigation of the underlying cellular and molecular mechanisms has focused on airway epithelial cell monoculture models, as well as direct exposure of cell types that are separated from the inhaled dose of diesel exhaust particulates *in vivo* by the epithelial barrier (Li *et al.*, 2008; United States Environmental Protection Agency, 2019). To address this knowledge gap, we tested the hypothesis that diesel exhaust particulate exposure causes transepithelial effects in human lung fibroblasts that reside beneath the bronchial epithelial barrier (Figure 1A) using a simple organotypic indirect coculture model (Figure 1B). Using this *in vitro* model, we compared the effects of direct diesel exhaust particulate exposure on a human bronchial epithelial cell barrier with its transepithelial effects on human lung fibroblasts in parallel over a time course.

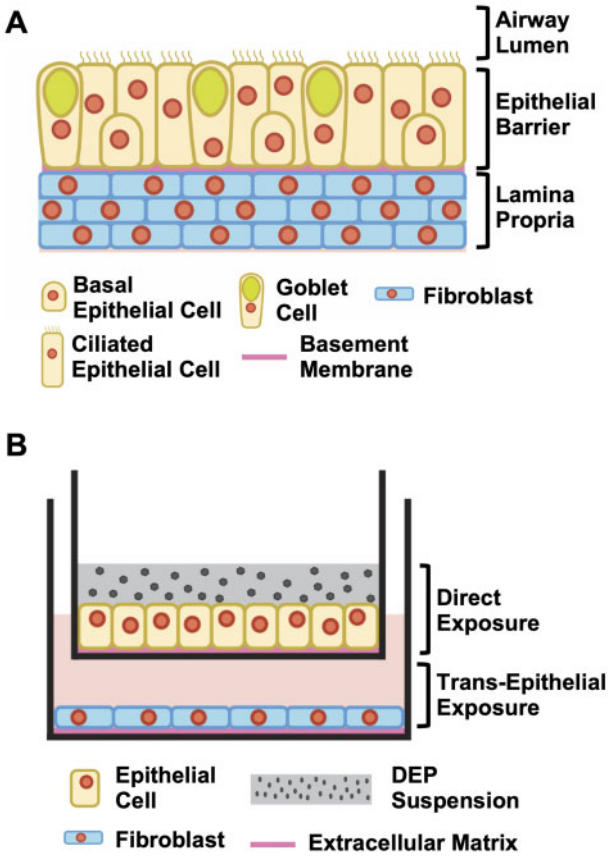

Figure 1. Transepithelial exposure model. A, Illustrated representation of the structure of the human bronchial epithelium and underlying lung fibroblasts *in vivo*. B, Schematic representation of the *in vitro* transepithelial exposure model demonstrating the difference between direct and transepithelial exposures. During transepithelial exposures, bronchial epithelial cells received direct exposure to diesel exhaust particulates (DEPs). In contrast, transepithelial exposure model fibroblasts were never in direct contact with the diesel exhaust and were only subject to transepithelial exposure.

MATERIALS AND METHODS

Preparation of diesel exhaust particulate suspensions. Whole diesel exhaust particulates (collection described by Sagai *et al.* [1993] and characterized as "A-DEP" by Singh *et al.* [2004]) were added to exposure media, consisting of Minimal Essential Medium with GlutaMAX (Life Technologies, No. 41090036) and 1% Penicillin/Streptomycin (Life Technologies, No. 15140-122), at 5 mg/ml prior to suspension by sonication on a Sonic Dismembrator Model 500 sonicator with microprobe tip (Fisher Scientific) for 4 cycles with the following parameters: 1 min per cycle, 0.9 s on, 0.1 s off, 30% output. The diesel exhaust particulate suspension was then diluted to 1 mg/ml in exposure medium and single-use stock aliquots were flash frozen in liquid nitrogen prior to storage at −80°C until further dilution in experiments. Aliquots from the diesel exhaust particulate resuspension batch were thawed, diluted to 100 μg/ml in exposure medium (described below), and agglomerate size distribution was determined by flow cytometric comparison with size

calibration standards (ThermoFisher No. F13838) to range primarily from 1 to 4 μm in diameter (Supplementary Figure 1).

Rationale for diesel exhaust particulate dosing. Inhaled particle dosimetry often describes the mean uniform deposition of particles within a defined region of the airway; however, particle deposition at bifurcation zones, which are adjacent to carinal ridges, of the tracheobronchial tree can be substantially greater than adjacent tubular wall regions (discussed in Martonen *et al.*, 1994). The resulting deposition enhancement factors range from approximately 330- to 2300-fold with 3- and 10-μm particles, respectively, under different ventilation rates and have been validated in humans *in vivo* (Balásházy *et al.*, 2003; Churg and Vedal, 1996; Zhang *et al.*, 2005). The enhanced deposition of inhaled particles at bifurcation zones corresponds to the incidence of bronchogenic tumors indicating an association between enhanced deposition at bifurcation zones/carinal ridges and adverse inhalation exposure outcomes (Martonen, 1992; Schlesinger and Lippmann, 1972, 1978).

An applied dose of 20 $\mu g/cm^2$ is approximately equivalent to the deposition of 2.5-μm-diameter particles at bifurcation zones within tracheobronchial generations 3–5 during light physical activity (15 l/min ventilation) over an 8 h exposure to an ambient particle concentration of 75 $\mu g/m^3$. This ambient exposure level is frequently exceeded in "real world" exposure scenarios in urban areas around the world. We used the Multi-Path Particle Dosimetry Model version 3.04 (Applied Research Associates, Inc) to calculate the mean deposited particle mass per surface area per breath under light activity (15 l/min ventilation) for airway generations 3–5 to be approximately 0.075 $\mu g/m^2$ per breath (Supplementary Figure 2) with the following parameters: Yeh/Schum 5-lobe model for constant exposure to 2.5-μm-diameter particles at an ambient concentration of 75 $\mu g/m^3$ with the nasal breathing scenario, 15 breaths/min, 1000 ml tidal volume, 0.5 inspiratory fraction, 0 pause fraction, upright orientation, default clearance parameters. The agglomerate size distribution in our diesel exhaust particulate suspension were approximately evenly distributed from 1 to 4 μm in diameter (Supplementary Figure 1), thus we used a mean particle diameter of 2.5 μm in dosimetry calculations. Inhaled particle deposition is greatly increased at bifurcation zones/carinal ridges and these areas also exhibit greater incidence of adverse inhalation exposure outcomes (Martonen, 1992; Schlesinger and Lippmann, 1972, 1978). The mean uniform deposition value obtained from the model was then multiplied by a deposition enhancement factor of approximately 350-fold to represent the increased deposition of 3-μm particles at airway bifurcations observed in several independent studies (Balásházy *et al.*, 2003; Churg and Vedal, 1996; Zhang *et al.*, 2005).

Determination of mean uniform particle mass deposition per surface area (m^2) within target tracheobronchial generations per hour:

$$0.075\frac{\mu g}{m^2 * breath} * 15\frac{breaths}{min} * 60\frac{min}{h} = 67.5\frac{\mu g}{m^2 * h}.$$

Conversion of surface area from m^2 to cm^2:

$$67.5\frac{\mu g}{m^2 * h} * \frac{10^{-4} m^2}{cm^2} = 0.00675\frac{\mu g}{cm^2 * h}.$$

Determination of total particle mass deposited per surface area (cm^2) over 8 h:

$$0.00675\frac{\mu g}{cm^2 * h} * 8\ h = 0.054\frac{\mu g}{cm^2}.$$

Determination of deposition per surface area at bifurcation zones/carinal ridges by multiplying mean uniform deposited particle mass by deposition enhancement factor:

$$0.054\frac{\mu g}{cm^2} * 350 = 18.9\ \frac{\mu g}{cm^2}.$$

Alternatively, our *in vitro* dose would also be equivalent to analogous deposition at rest (7.5 l/min ventilation) for 8 h at an ambient particle concentration of 175 $\mu g/m^3$ (additional calculations in Supplementary Materials).

Chemical reagents. Hydrogen peroxide (H_2O_2) (30% w/v) (No. H1009), DL Dithiothreitol (DTT) (No. D9779), N-acetyl-L-cysteine (NAC) (No. A9165), catalase (CAT) from bovine liver (No. C1345), and L-ascorbic acid (AA) (No. A4403) were obtained from Sigma Aldrich and indicated as cell culture grade.

Cell culture. The human bronchial epithelial cell line16HBE4o− (hereafter referred to as "bronchial epithelial cells") (Cozens *et al.*, 1994; Feng *et al.*, 2015) was generously provided by Dr Ilona Jaspers at the University of North Carolina (UNC) at Chapel Hill and harvested from exposures at adjusted population doubling 4–40 (assignment of adjusted population doubling from passage number is described in Supplementary Methods). Bronchial epithelial cells were maintained in complete bronchial epithelial cell growth medium ([minimum essential medium with GlutaMAX; Life Technologies, No. 41090036] supplemented with 10% fetal bovine serum [Life Technologies, No. 16000-044] and 1% Penicillin/Streptomycin [Life Technologies, No. 15140-122]) as described in McNabb and McCullough (2019b). The human lung fibroblast cell line IMR90 (hereafter referred to as "lung fibroblasts") (Nichols *et al.*, 1977) was obtained from the American Type Culture Collection (ATCC, No. CCL-186), cultured in lung fibroblast growth medium (minimum essential medium with GlutaMAX supplemented with 10% fetal bovine serum, nonessential amino acids, and 1% Penicillin/Streptomycin) as described in McNabb and McCullough (2019c). Lung fibroblasts were used in exposure experiments at adjusted population doubling range of 6–25. Primary human bronchial epithelial cells (hereafter referred to as "primary bronchial epithelial cells") were obtained from via bronchial brushing from 3 healthy nonsmoking volunteers (donor information in Supplementary Table 1). Donors gave their informed consent after being informed of risks and procedures. The protocol and consent form were approved by the UNC School of Medicine Committee on the Protection of the Rights of Human Subjects and by the U.S. Environmental Protection Agency. Primary bronchial epithelial cells were expanded in Pneumacult Ex-Plus (STEMCELL Technologies, No. 05040) and seeded on 12-mm Transwell inserts prior to differentiation during air-liquid interface culture in PneumaCult-ALI Medium (STEMCELL Technologies, No. 05001) for 21–30 days. Primary normal human lung fibroblasts (hereafter referred to as "primary lung fibroblasts") ($n = 3$ donors) were generously provided by Dr Scott Randell of the University of North Carolina at Chapel Hill Cystic Fibrosis/Pulmonary Research and Treatment Center Tissue Procurement Core and cells from an adjusted population doubling range of 7–12 were used in experiments and maintained in complete lung fibroblast growth medium (donor information in Supplementary Table 1). Cells were incubated at 37°C with 5% CO_2 and 20% O_2 and passaged every 3 days onto tissue culture

plates coated with bovine type I collagen solution (Advanced BioMatrix, No. 5005) as described in McNabb and McCullough (2019a). Bronchial epithelial cells and lung fibroblasts were assessed by STR profiling (results included in Supplementary Materials) and tested negative for *Mycoplasma* spp. contamination.

Transepithelial exposure model. As shown in Supplementary Figure 3, bronchial epithelial cells were seeded at a density of 3.33 $\times$ 10^5 or 3.42 $\times$ 10^5 cells/cm^2 onto collagen-coated 12- or 24-mm Transwell inserts with a 0.4 μm pore size (Corning, No. 3460 and 3524), respectively, and lung fibroblasts or primary lung fibroblasts were seeded at 2.63 $\times$ 10^4 or 2.10 $\times$ 10^4 cells/cm^2 on collagen-coated 12- or 6-well plates (Corning), respectively, on day 1. All cells were seeded in their respective growth medium. On day 2, cells were combined in coculture by adding the bronchial epithelial cell-seeded Transwell insert (apical compartment) into the multiwell fibroblast-seeded plate (basolateral compartment). On day 3, diesel exhaust particulates aliquots were thawed and diluted to 100 μg/ml in exposure medium and the apical medium was replaced with exposure medium alone (vehicle) or a diesel exhaust particulate suspension sufficient to achieve a dose of 20 μg/cm^2 (rationale described above), which is similar or lower than doses used in comparable *in vitro* studies (Baulig *et al.*, 2003; Danielsen *et al.*, 2008; Ji *et al.*, 2018; Mazzarella *et al.*, 2007; Rynning *et al.*, 2018). In transepithelial exposure model experiments utilizing primary bronchial epithelial cells, inserts containing differentiated cells in air-liquid interface culture were transferred into wells containing lung fibroblasts that had been plated 2 days earlier. Diesel exhaust particulate suspension was then added to primary bronchial epithelial cells in a manner consistent with bronchial epithelial cell transepithelial exposures as described above. Apical and basolateral compartments were separated for cell-specific analysis of the indicated endpoints immediately following the indicated exposure durations. A detailed protocol for set-up and exposure experiments using the transepithelial exposure model is available on the Nature Research Protocol Exchange (McNabb *et al.*, 2019). Here, we use the term "direct"/"direct exposure" to describe direct contact with the full diesel exhaust particulate dose applied to bronchial epithelial cells. Fine and ultrafine particles have been reported to translocate across the airway epithelial barrier and thus may come into contact with lung fibroblasts and/or other cell types; however, the potential interactions of lung fibroblasts with translocated diesel exhaust particulates were considered to be a component of "transepithelial" exposures in this study.

Transepithelial electrical resistance assay. Bronchial epithelial cells seeded in 12 mm Transwell inserts and cultured in the transepithelial exposure model and exposed to vehicle or 20 μg/cm^2 diesel exhaust particulates for 24 h. Bronchial epithelial cell-seeded inserts were then placed in new multiwell plates prior to measuring electrical resistance (Ω*cm^2) across the bronchial epithelial cell monolayer using an Epithelial Voltohmmeter (EVOM2; World Precision Instruments, Inc) as described in Faber *et al.* (2019). Resistance measurements for blank wells were subtracted and the corrected resistance values were then multiplied by the insert surface area (Srinivasan *et al.*, 2015). Three measurements were taken per insert and values represent the mean of 3 inserts in each of 4 independent exposures ± SD.

Fluorescein isothiocyanate-labeled dextran assay. Bronchial epithelial cell-seeded in 12 mm Transwell inserts were cultured in the transepithelial exposure model and exposed to vehicle or 20 μg/cm^2 diesel exhaust particulates for 24 h prior to determination of transepithelial permeability to 20 kDa fluorescein isothiocyanate (FITC)-labeled dextran (Sigma, No. FD20) as described in Faber and McCullough (2019).

Immunofluorescent staining. Bronchial epithelial cell-seeded in 12 mm Transwell inserts were cultured in the transepithelial exposure model for 24 h. Transwell inserts were then placed in new multiwell plates prior to fixation in 4% paraformaldehyde (Electron Microscopy Sciences, No. 15710), blocked with normal donkey serum (Jackson ImmunoResearch, No. 017-000-121), and incubated with α-zona occludens 1 (ZO-1; Cell Signaling Technology, No. 5406) or α-E-cadherin (E-cad; Cell Signaling Technology, No. 3195) overnight at 4°C. Cells were washed and incubated with donkey α-Rabbit IgG secondary antibody (Jackson ImmunoResearch, No. 711-005-152) and Alexa Fluor 488 donkey α-rabbit IgG (H + L) (Life Technologies No. A21206) overnight at 4°C. Cells were then stained with Hoechst 33342 (Life Technologies, No. H3570) and Alexa Fluor 594 Phalloidin (Life Technologies, No. A1238). Antibody dilutions are listed in Supplementary Table 3. The membrane was cut out of the insert and mounted with Molecular Probes ProLong Gold Antifade Mountant (Life Technologies) on a microscope slide with No. 1.5 coverslips. Cells were imaged after 24 h on a Zeiss LSM 710 Spectral Confocal Laser Scanning Microscope (Jena, Germany). We used a Plan-Apochromat 63 $\times$ /1.40 Oil DIC objective with X1.8 zoom and 600 $\times$ 600 pixels, for an effective pixel size of 0.128 μm. Excitation lasers were 405 nm (for Hoechst), 488 nm (for AlexaFluor 488), and 594 nm (for AlexaFluor 594). Emission filter windows were 415–474 (for DAPI), 504–562 (for AlexaFluor 488), and 604–670 (for AlexaFluor 594).

Measurement of glutathione redox homeostasis and intracellular H_2O_2. The lentiviral dual-fluorescent reactive oxygen species/oxidized glutathione biosensor (pLV-dfROX, Addgene No. 137170) was constructed by generating and inserting a bicistronic expression cassette containing the redox-sensitive biosensors roGFP2 and HyPer Red into pSDM101 (McCullough *et al.*, 2012) by PCR amplification from an intermediate vector constructed following the excision of roGFP2 and HyPer Red from pTLRED-roGFP2 (Cheng *et al.*, 2012) and pC1-HyPer-Red (Addgene No. 48249), respectively (primer sequences listed in Supplementary Table 3). All plasmid transformations were conducted in *Escherichia coli* strain HB101. Recombinant lentiviral particles were generated using the pLV-dfROX lentiviral transfer vector as described by McCullough (2019). To quantify relative changes in global cellular glutathione redox state and intracellular H_2O_2 levels, lung fibroblasts were seeded (1 $\times$ 10^5 cells/ml) on human collagen/fibronectin-coated (type I human collagen [Advanced BioMatrix, No. 5005], fibronectin human plasma [Sigma Aldrich, No. F2006], bovine serum albumin [Sigma Aldrich, No. A7906], and LHC basal media [Life Technologies, No. 12677019]) glass bottom plates (MatTek), and bronchial epithelial cells were seeded (1 $\times$ 10^6 cells/ml) in collagen-coated 24-mm Transwell inserts for 24 h. Lung fibroblasts were transduced as described by Faber *et al.* (2020) approximately 30 h after seeding with pLV-dfROX viral particles (multiplicity of infection of 3) and 2 μg/ml polybrene solution in complete lung fibroblast growth medium overnight. Lung fibroblasts were washed 3 times with Dulbecco's phosphate buffered saline then changed into phenol red-free complete lung fibroblast growth medium. Bronchial epithelial cell medium was changed to phenol red-free complete bronchial epithelial cell growth medium, and the bronchial epithelial cells were combined in coculture with the lung fibroblasts. After 24 h, cells were imaged on an Olympus IX81 Inverted Light

Microscope (Tokyo, Japan) with a PlanApoN 60X/1.42 oil objective within a Tokai Hit Microscope Stage Top Incubator (Tokai Hit Co, Ltd) with 5% CO_2 and over 90% humidity. The detector was a Hamamatsu sCMOS Flash 4 V2 camera, with pixels binned 4 × 4, for an effective pixel size of 0.427 μm. Treatment-induced accumulation of intracellular reactive oxygen species (ie, H_2O_2) leads to the oxidation of glutathione, which was measured as changes in the ratio of fluorescent light emitted by the roGFP2 biosensor when excited with an X-Cite Xylis XT720L (385) LED using a 387/11-nm excitation filter (oxidized state) or a 485/20-nm excitation filter (reduced state) (Hanson *et al.*, 2004). In both cases, the resulting fluorescence was collected using a 525/30-nm emission filter. Images were acquired every 3 min, at multiple positions, and focus was maintained throughout the experiment with hardware-based autofocus (Olympus ZDC). HyPer Red fluorescence (excited with a 560/25-nm filter and collected with a 607/36-nm filter) increases in concert with the accumulation of intracellular H_2O_2 (Ermakova *et al.*, 2014). Diesel exhaust particulates were injected into the apical compartment via BD Biosciences intramedic polyethylene 0.030-inch inner diameter tubing (No. 427416), and lung fibroblasts received transepithelial diesel exhaust particulate exposure for 6 h. Based on previous studies with roGFP2 (Cheng *et al.*, 2012; Gibbs-Flournoy *et al.*, 2013; Wages *et al.*, 2014), transepithelial diesel exhaust particulate response data in lung fibroblasts were normalized to maximal roGFP2 and HyPer Red signal with the injection of 1 mM H_2O_2 directly to the lung fibroblasts after 6 h for 9 min. Reversal of roGFP2 and HyPer Red signal was then demonstrated with the injection of 10 mM DTT directly to lung fibroblasts for an additional 9 min. Description of live cell imaging data analysis with pLV-dfROX can be found in the Supplementary Methods.

Quantitative real-time polymerase chain reaction. RNA was extracted from lysed samples using an RNA Mini Kit (Life Technologies) as described in McNabb and McCullough (2020) and quantified using a Nanodrop OneC Spectrophotometer (ThermoFisher Scientific, Waltham, Massachusetts). One microgram was used to synthesize cDNA using the iScript Reverse Transcription kit (Bio-Rad, Hercules, California, No. 1708891) according to the manufacturer's protocol. Fold change in transcript abundance was assessed using multiplexed primers and hydrolysis probes (sequences listed in Supplementary Table 2) in technical triplicates on a CFX96 Touch (Bio-Rad). Target gene C_q values were normalized to matched β-actin (ACTB) C_q values and expressed as fold changes between vehicle and diesel exhaust particulate exposure treatments using the Pfaffl method (Pfaffl, 2001).

Oxidative stress and antioxidant response qPCR array. Two micrograms of isolated RNA was used to synthesize cDNA using the iScript Reverse Transcription kit (Bio-Rad). cDNA from technical triplicates of each exposure replicate was pooled and assessed using PrimePCR Oxidative Stress and Antioxidant Defense Plus (SAB Target List) H96 arrays (Bio-Rad, No. 10040245), which were run on a CFX96 Touch Real Time PCR Detection System (Bio-Rad). Gene expression was normalized to *HPRT1* and fold changes were determined using the $\Delta\Delta C_t$ method.

Western blotting. Cellular extracts were prepared in RIPA buffer (50 mM Tris, pH 8.0; 150 mM NaCl; 1% Triton X-100; 400 μM EDTA; 10% glycerol; 0.1% SDS; 0.1% deoxycholate) with protease (complete EDTA-free, Roche) and phosphatase (PhosSTOP, Roche) inhibitors. Cellular debris was removed via centrifugation and aliquots of RIPA extract were removed for protein quantification via BCA assay (ThermoFisher, No. 23222). The remaining supernatant was supplemented with 5X Laemmli loading buffer (250 mM Tris, pH 6.8; 500 mM DTT; 50% glycerol; 10% SDS; 0.5% bromophenol blue), incubated at 95°C for 5 min, aliquoted, and stored at −80°C. For each sample, equal amounts of protein were loaded into SDS-PAGE gels, electrophoresed, and transferred to 0.45 μm pore nitrocellulose membranes (Bio-Rad, No. 1620115) via wet transfer. Following primary antibody binding, horseradish peroxidase-conjugated secondary antibodies (Jackson ImmunoResearch, No. 711-036-152), and Pierce Enhanced Chemiluminescence Western blotting substrate (ThermoFisher) were used to generate chemiluminescence. Immunoblots were imaged on a ChemiDoc MP Imaging System (Bio-Rad). The antibodies used for this analysis were all obtained from Cell Signaling Technologies: α-NRF2 (No. 12721), α-HMOX1 (No. 82206), α-NQO1 (No. 62262), α-PTGS2 (No. 12282), α-p62/SQSTM1 (No. 8025), α-GAPDH (No. 5174), and α-cyclophilin B (No. 43603). Stabilization of NRF2 was determined by increased intensity of the approximately 95–110 kDa band as indicated by the manufacturer and previous studies (Kemmerer *et al.*, 2015; Lau *et al.*, 2013). Densitometry was performed using FIJI by ImageJ (Schindelin *et al.*, 2012) and genes were normalized to either α-GAPDH or α-cyclophilin B as reference genes and expressed as a comparison with unexposed cells. Specific Western blotting details can be found in Supplementary Tables 3 and 4.

Statistical analysis. All statistical analyses were conducted using GraphPad Prism 8.02 (GraphPad Software). Transepithelial electrical resistance, FITC-dextran, and the effect of antioxidant treatment were analyzed for statistical significance by 1-way ANOVA with Sidak's multiple comparison test. Statistical significance of gene expression (RNA and protein) was determined by 2-way ANOVA with multiple test comparisons by Tukey's test. A p value of $\leq .05$ was considered statistically significant for all analyses.

RESULTS

In Vivo *Barrier Characteristics of Epithelial Cell Layer in the Transepithelial Exposure Model*

Functional epithelial barriers are characterized by the formation of tight and adherens junctions, increase in transepithelial electrical resistance, and impermeability to low molecular weight compounds, such as 20 kDa FITC-dextran (FITC-dextran-20) (Lehmann *et al.*, 2009; Saatian *et al.*, 2013). Immunofluorescent (IF) staining of transepithelial exposure model bronchial epithelial cells demonstrated the colocalization of phalloidin-stained actin filaments with both ZO-1 and E-cad at cell-cell junctions (Figure 2A), which is consistent with the formation of an intact epithelial cell barrier (Gonzalez-Mariscal *et al.*, 2011; Itoh and Bissell, 2003). The presence of these structural aspects of an epithelial barrier was complemented by an increase in transepithelial exposure model bronchial epithelial cell layer electrical resistance compared with insert alone (Figure 2B). The diffusion of 20 kDa FITC-dextran across the transepithelial exposure model bronchial epithelial cell layer was not statistically different from the fluorescence of medium alone but was significantly less than that observed in the absence of an bronchial epithelial cell layer (Figure 2C). The reported effects of diesel exhaust particulate treatment on transepithelial electrical resistance at equal or slightly higher doses varies in other studies (Bayram *et al.*, 1998; Lehmann *et al.*, 2009); however, 24 h diesel exhaust particulate treatment did not significantly affect either the electrical resistance or permeability of the transepithelial exposure model bronchial epithelial layer to 20 kDa FITC-dextran (Figs. 2B and 2C).

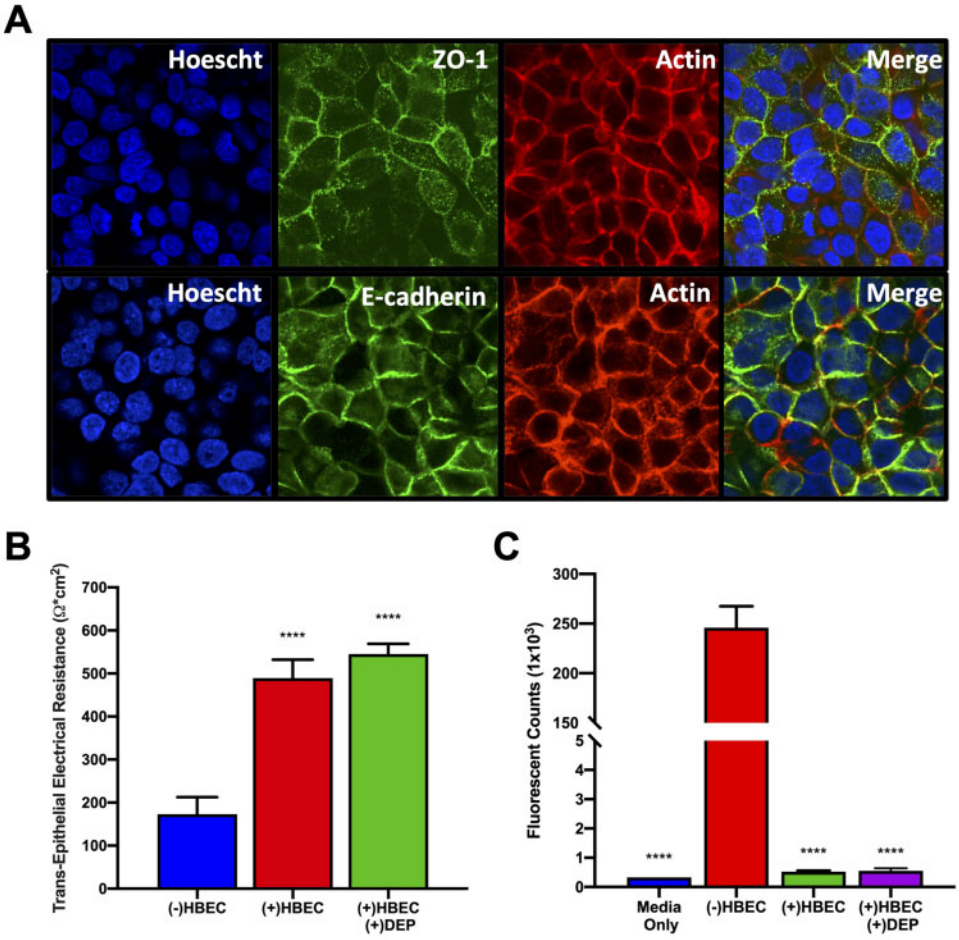

Figure 2. Transepithelial exposure model bronchial epithelial cell (HBEC) layer exhibits epithelial barrier function. To test HBEC barrier permeability, integrity, and expression of known epithelial markers, HBECs were seeded in Transwell inserts and combined with lung fibroblasts within the transepithelial exposure model for 24 h. A, After 24 h in the transepithelial exposure model, HBECs exhibited ZO-1 and E-cadherin-positive tight and adherens junctions, respectively, that colocalized with actin staining on the cellular periphery. Images were acquired with a X63 objective. B, The transepithelial exposure model HBEC layer formed an electrically resistant and (C) low molecular weight impermeable barrier. Exposure to 20 μg/cm^2 diesel exhaust particulates (DEPs) for 24 h did not alter either electrical resistance or epithelial barrier permeability. Values represent the mean of 4 independent experiments ± SD and statistical significance of $p \leq .0001$ relative to insert without HBEC monolayer is represented by (****) in B and C.

Cytotoxicity of Direct and Transepithelial Diesel Exhaust Particulate Exposures

To ensure that the effects of direct and transepithelial diesel exhaust particulate exposures on bronchial epithelial cells and lung fibroblasts, respectively, were not artifacts associated with cytotoxicity, we assessed cell viability following 24 h diesel exhaust particulate exposure in both cell types. Neither direct nor transepithelial diesel exhaust particulate exposures caused a significant change in the percentage of live bronchial epithelial cells or lung fibroblasts, respectively (Supplementary Figure 4).

Live Cell Imaging of Fluorescent Biosensors for Intracellular H_2O_2 Accumulation and Glutathione Oxidation in Transepithelial Diesel Exhaust Particulate-exposed Lung Fibroblast

Direct exposure to diesel exhaust particulates results in the intracellular accumulation of hydrogen peroxide (Steiner *et al.*, 2016) and oxidation of cellular glutathione (Cheng *et al.*, 2012; Gibbs-Flournoy *et al.*, 2013; Wages *et al.*, 2014), a surrogate for global cellular redox balance, in bronchial epithelial cells; however, to our knowledge, the ability of transepithelial diesel exhaust particulate exposure to alter redox balance within cells beyond the epithelial barrier (ie, stromal cells) has not yet been investigated. We generated a recombinant lentiviral vector (pLV-dfROX) expressing dual fluorescent biosensors for glutathione oxidation (roGFP2) (Hanson *et al.*, 2004) and hydrogen peroxide (HyPer Red) (Ermakova *et al.*, 2014) to quantify glutathione oxidation and hydrogen peroxide accumulation simultaneously in real time by live cell imaging of transduced transepithelial exposure model lung fibroblasts (Figure 3A). Transepithelial diesel exhaust particulate exposure led to a steady increase in both HyPer Red fluorescence and the roGFP2 ratio of 387/485 nm fluorescence intensity over 360 min of exposure, indicating both an increase in intracellular hydrogen peroxide and oxidation of the roGFP2 biosensor (Figs. 3B and 3C). Transepithelial diesel exhaust particulate exposure of lung fibroblasts resulted in HyPer Red fluorescence intensity and roGFP2 405/488 nm ratio of 90.7% (±6.3%) and 83.0% (±9.3%) of values obtained by direct exposures to 1 mM hydrogen peroxide, respectively (Figs. 3B and 3C).

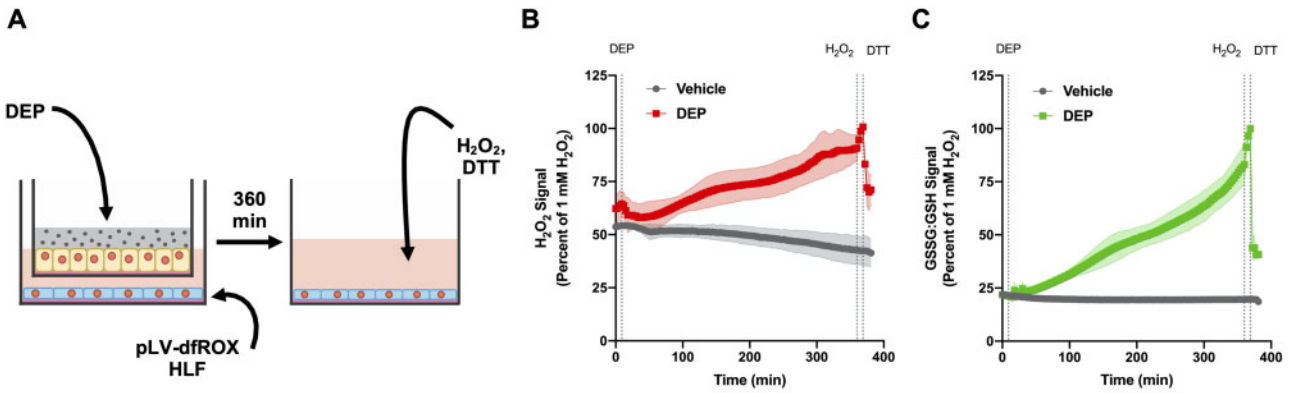

Figure 3. Real-time dual redox biosensor live cell imaging identifies transepithelial diesel exhaust particulate (DEP)-induced redox dysfunction. Lung fibroblasts were transduced with lentiviral dual-fluorescent reactive oxygen species/oxidized glutathione biosensor (pLV-dfROX) lentiviral particles. After 24-h lung fibroblasts were washed, media were changed to phenol red-free, and bronchial epithelial cell (HBEC)-containing insert was added to lung fibroblast cultures. A, Graphical depiction of live cell imaging protocol. DEPs were added to the HBEC barrier while live cell imaging data were acquired in underlying lung fibroblasts for 360 min. The DEP exposure was stopped by removal of the Transwell insert. Hydrogen peroxide (1 mM final concentration) was then added directly to the remaining medium and lung fibroblasts for 9 min to obtain peak signal for both biosensors. Reversal of roGFP2 and HyPer Red signal was then demonstrated with the injection of dithiothreitol (DTT) (10 mM final concentration) directly to lung fibroblasts for an additional 9 min. B, Transepithelial DEP exposure causes an increase in HyPer Red fluorescence indicating the accumulation of intracellular hydrogen peroxide over a 360 min exposure duration. C, Transepithelial DEP exposure increases the ratio of roGFP2 fluorescence emission following excitation around 387 nm compared with that observed following excitation around 485 nm, indicating an increase in oxidized cellular glutathione. Values presented in B and C are expressed relative to the signal observed following direct treatment of lung fibroblasts with hydrogen peroxide (1 mM final concentration). Data represent $n = 2$ exposure replicates for vehicle and $n = 4$ transepithelial DEP exposure replicates with SD of an average of 18 fields of view per replicate. Abbreviation: HLFs, lung fibroblasts.

Expression of Oxidative Stress-Responsive Genes in Bronchial Epithelial Cells and Lung Fibroblasts Following Direct and Transepithelial Diesel Exhaust Particulate Exposure, Respectively

Initially, we determined the kinetics of transepithelial diesel exhaust particulate-mediated induction of the sentinel oxidative stress-responsive gene heme oxygenase 1 (*HMOX1*) in lung fibroblasts. *HMOX1* transcript was elevated in transepithelial diesel exhaust particulate-exposed lung fibroblasts, relative to vehicle, at all timepoints evaluated with peak induction at 6 h of exposure (Figure 4A). Observations in lung fibroblasts were validated using primary lung fibroblasts from 3 donors, which all exhibited patterns of *HMOX1* transcript induction that were not significantly different from lung fibroblasts (Figure 4A). We conducted further validation by assessing the transepithelial diesel exhaust particulate-mediated induction of HMOX1 in lung fibroblasts following the replacement of bronchial epithelial cells in the transepithelial exposure model with primary bronchial epithelial cells that had undergone mucociliary differentiation during air-liquid interface culture. Lung fibroblasts subjected to transepithelial diesel exhaust particulate exposure in this model exhibited similar magnitude of *HMOX1* transcript induction at 6 and 24 h (relative to lung fibroblasts cocultured with bronchial epithelial cells) (Supplementary Figure 5).

We further characterized the induction of oxidative stress-responsive genes in fibroblasts at 6 h of transepithelial diesel exhaust particulate exposure using a quantitative real-time polymerase chain reaction (qPCR) array with 90 oxidative stress response and antioxidant defense target genes. Transepithelial diesel exhaust particulate exposure alternatively regulated 13 target genes in lung fibroblasts (Supplementary Figure 6), which were also alternatively regulated in primary lung fibroblasts from all 3 donors (Figure 4B). To validate qPCR array results and further investigate the kinetic profiles of alternatively regulated genes in transepithelial diesel exhaust particulate-exposed fibroblasts, we performed targeted time-course gene expression analyses with additional oxidative stress-responsive genes, NAD(P)H quinone dehydrogenase 1 (*NQO1*), prostaglandin-endoperoxide synthase 2 (*PTGS2*), and protein 62/sequestosome 1 (*SQSTM1*). The transcripts of the 3 additional target genes were upregulated in both transepithelial diesel exhaust particulate-exposed lung fibroblasts and primary lung fibroblasts. The abundance of *HMOX1* and *PTGS2* transcripts exhibited an early response with peak induction at 6 h or between 4 and 6 h, respectively. In contrast, *NQO1* and *SQSTM1* both exhibited a later response with peak transcript induction occurring at 24 h (Figure 4A). Despite the direct and transepithelial nature of bronchial epithelial cell and lung fibroblast diesel exhaust particulate exposure in the transepithelial exposure model, respectively, the kinetics and magnitudes of *HMOX1*, *NQO1*, *PTGS2*, and *SQSTM1* transcript induction were not statistically different between the 2 cell types with the exception of *HMOX1* at 6 and 8 h and *NQO1* at 24 h (Figure 4A). To confirm oxidative stress-responsive gene expression at the protein level, we performed time-course immunoblotting for HMOX1, NQO1, PTGS2, and SQSTM1 proteins in both lung fibroblasts and bronchial epithelial cells. The induction kinetics of all 4 target proteins were similar to their respective transcripts with the exception of PTGS2 protein, which was not induced in bronchial epithelial cells and remained elevated from 6 to 24 h in lung fibroblasts (Figs. 4C and 4D). Following 24 h of exposure, HMOX1 and SQSTM1 proteins remained significantly elevated in bronchial epithelial cells whereas NQO1, PTGS2, and SQSTM1 remained significantly elevated in lung fibroblasts.

Activation of NRF2 in Bronchial Epithelial Cells and Lung Fibroblasts Following Direct and Transepithelial Diesel Exhaust Particulate Exposure, Respectively

Eleven of the 13 genes identified as being alternatively regulated in transepithelial diesel exhaust particulate-exposed lung

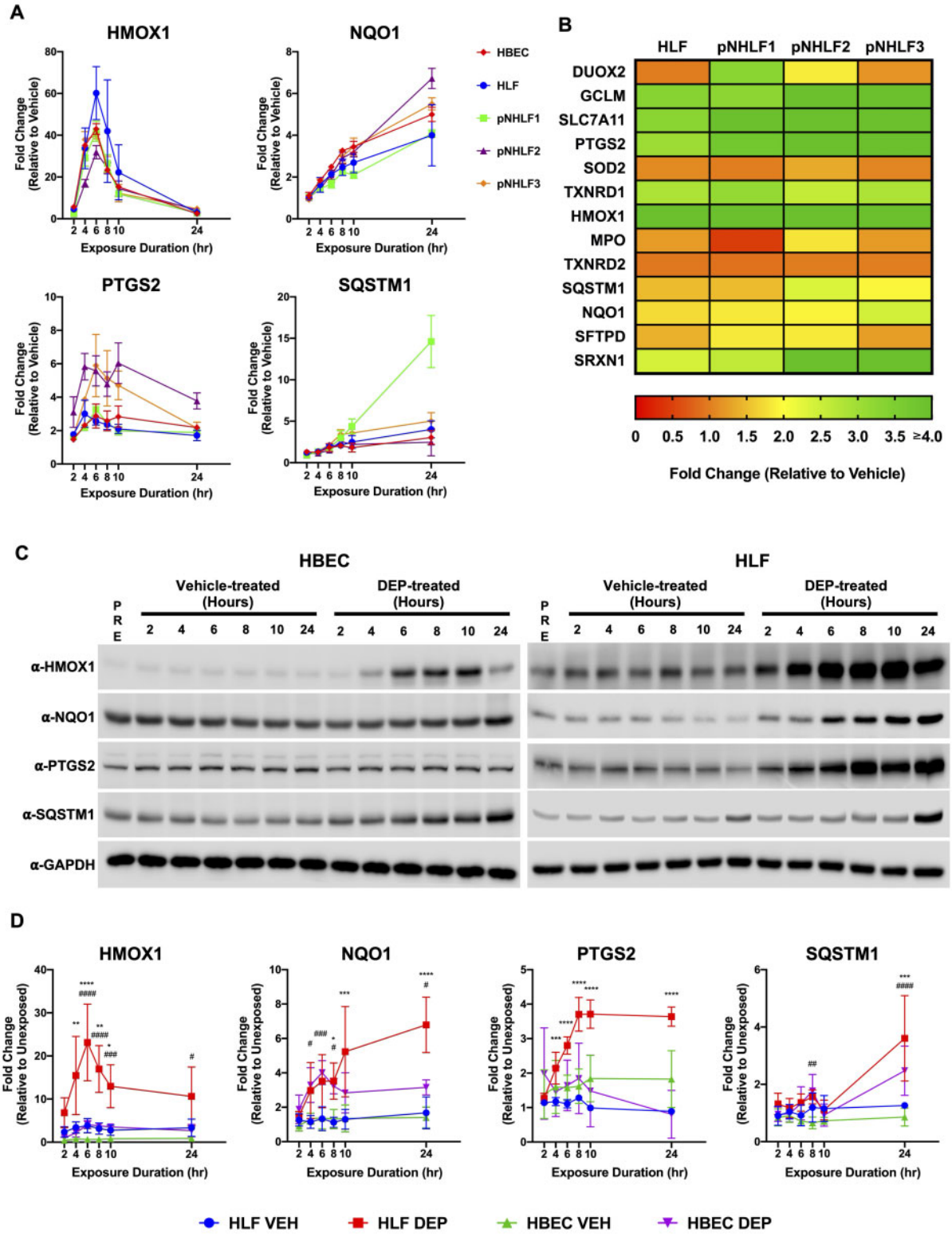

Figure 4. Oxidative stress-responsive gene signaling is activated in lung fibroblasts (HLFs) and bronchial epithelial cells (HBECs) following transepithelial diesel exhaust particulate (DEP) exposure. HBEC ($n = 5$), HLFs ($n = 5$), and primary lung fibroblasts (pNHLF; $n = 3$ donors) were harvested following 2–24 h of exposure to vehicle (VEH) or DEPs within the transepithelial exposure model. A, Direct and transepithelial DEP-induced mRNA expression of the oxidative stress-responsive genes *HMOX1*, *NQO1*, *PTGS2*, and *SQSTM1* in HBECs and HLFs/pNHLFs, respectively. B, Induction of oxidative stress and antioxidant defense mRNA expression following 6 h of transepithelial DEP exposure in HLFs (mean of 3 independent experiments shown) and pNHLFs from 3 donors. Values indicate fold change of DEP samples relative to vehicle controls following normalization to *HPRT1*. C, Immunoblots showing protein levels of exposure-induced target gene expression in direct and transepithelial DEPs exposed HBECs and HLFs, respectively. The immunoblots shown are representative of results obtained from 3 independent replicate exposures. D, Densitometry performed with FIJI for ImageJ and normalized to unexposed ("PRE") HBECs or HLFs, respectively. Significant differences between vehicle or transepithelial DEP-treated HLFs ($n = 4$) are indicated by $^{*}p \leq .05$, $^{**}p \leq .01$, $^{***}p \leq .001$, and $^{****}p \leq .0001$. Significant differences between vehicle and DEP-treated HBECs ($n = 3$) are indicated by $^{\#}p \leq .05$, $^{\#\#}p \leq .01$, $^{\#\#\#}p \leq .001$, and $^{\#\#\#\#}p \leq .0001$. Values represent the mean ± SD.

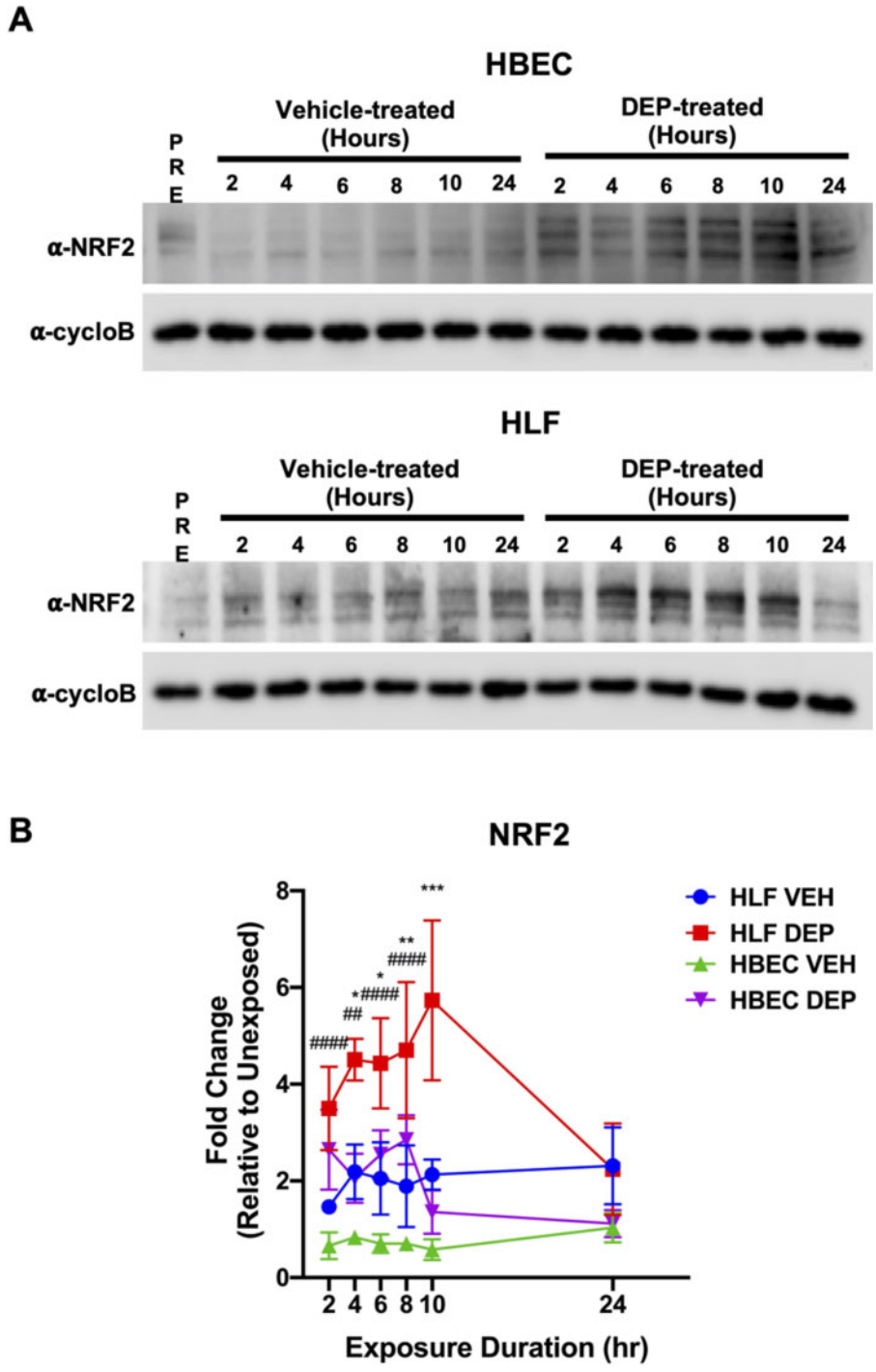

Figure 5. NRF2 is stabilized in bronchial epithelial cells (HBECs) and lung fibroblasts (HLF) following transepithelial diesel exhaust particulate (DEP) exposure. Whole cell lysates from vehicle (VEH) and DEP exposed (A) HBECs and HLFs were immunoblotted with antibodies that specifically recognize NRF2 and cyclophilin B (loading control). The immunoblots shown are representative of results obtained from 3 independent replicate exposures. B, Densitometry performed with FIJI for ImageJ and normalized to unexposed HBECs or HLFs, respectively. Significant differences between vehicle or transepithelial dieselexhaust particulate treated lung fibroblasts ($n = 4$) are indicated by $^{*}p \leq .05$, $^{**}p \leq .01$, and $^{***}p \leq .001$. Significant differences between vehicle and diesel exhaust particulate treated bronchial epithelial cells ($n = 3$) are indicated by $^{\#\#}p \leq .01$ and $^{\#\#\#\#}p \leq .0001$. Values represent the mean ± SD.

fibroblasts and primary lung fibroblasts in qPCR arrays are regulated by the oxidative stress-responsive transcription factor, nuclear factor, erythroid 2 like 2 (NRF2; NFE2L2). To define the kinetic relationship between transepithelial diesel exhaust particulate exposure, oxidative stress-responsive signaling events, and oxidative stress/antioxidant gene induction we conducted time-course immunoblotting for NRF2 stabilization, which is an indicator of NRF2 pathway activation (Nguyen *et al.*, 2009). Transepithelial exposure model diesel exhaust particulate exposure resulted in significant stabilization of NRF2 protein in bronchial epithelial cells from 2 to 8 h and from 4 to 10 h in lung fibroblasts (Figure 5).

Effects of Targeted Antioxidant Treatment of Lung Fibroblasts on Diesel Exhaust Particulate-induced Oxidative Stress-Responsive Gene Expression

Diesel exhaust particulates cause redox imbalance (eg, reactive oxygen species formation), which can be mitigated by the addition of antioxidants *in vitro* and *in vivo* (Baulig *et al.*, 2003; Han *et al.*, 2001). To determine whether transepithelial diesel exhaust particulate-dependent oxidative stress-responsive gene expression in lung fibroblasts was dependent on levels of reduced glutathione, antioxidant capacity, or hydrogen peroxide, we treated lung fibroblasts with N-acetylcysteine (NAC) (Carlsten *et al.*, 2014), L-ascorbic acid (AA) (Rodrigues da Silva *et al.*, 2018), and catalase (CAT) (Okubo *et al.*, 2015), respectively, prior to transepithelial diesel exhaust particulate exposure. To prevent the antioxidant treatments from directly impacting the bronchial epithelial cells, inserts were transferred to conditioned medium during the 1 h of antioxidant treatment of lung fibroblasts, after which the antioxidant-containing medium was removed and replaced with conditioned medium prior to the replacement of the insert (Figure 6A). Samples for transcriptional analyses were collected at 6 and 24 h of direct/transepithelial diesel exhaust particulate exposure, which correspond to peak induction of HMOX and PTGS2, and NQO1 and SQSTM1 transcripts, respectively (Figure 4A). Similarly, corresponding protein levels were analyzed at 8 and 24 h of direct/transepithelial diesel exhaust particulate exposure (Figs. 4C and 4D). Pretreatment of lung fibroblasts with all 3 antioxidants mitigated the transepithelial diesel exhaust particulate-mediated induction of *HMOX1* transcript but did not have significant effects on *NQO1*, *PTGS2*, or *SQSTM1*, in lung fibroblasts (Figure 6B). Pretreatment of lung fibroblasts with either N-acetylcysteine or ascorbic acid reduced the diesel exhaust particulate-mediated induction of *HMOX1*, *PTGS2*, *NQO1*, and *SQSTM1* transcripts in bronchial epithelial cells, whereas pretreatment with catalase affected *NQO1* transcript induction (Figure 6B). To confirm that antioxidant treatment mitigated transepithelial diesel exhaust particulate-induced oxidative stress-responsive gene expression at the protein level, we assessed protein levels of HMOX1 and PTGS2 at 8 h and NQO1 and SQSTM1 at 24 h in N-acetylcysteine-pretreated lung fibroblasts and adjacent bronchial epithelial cells following transepithelial and direct diesel exhaust particulate exposure, respectively. Pretreatment with N-acetylcysteine had a significant impact on the transepithelial diesel exhaust particulate-mediated induction of HMOX1, but not NQO1, PTGS2, or SQSTM1, protein in lung fibroblasts (Figs. 6C and 6D). Further, N-acetylcysteine pretreatment of lung fibroblasts significantly reduced the diesel exhaust particulate-mediated induction of HMOX1 and NQO1, but not PTGS2 and SQSTM1 protein in adjacent bronchial epithelial cells (Figs. 6C and 6D).

DISCUSSION

The adverse effects of air pollution exposures on cardiopulmonary health are linked to their ability to cause pulmonary oxidative stress resulting from both the direct oxidative effects of individual pollutants and their ability to induce the production of reactive oxygen species (Lodovici and Bigagli, 2011). The persistence of air pollution-induced pulmonary oxidative stress and associated pulmonary inflammation play an integral role in the development of both chronic pulmonary and systemic disease (Anderson *et al.*, 2012; Rao *et al.*, 2018; Valavanidis *et al.*, 2013). Pulmonary oxidative stress is also a key pathway in respiratory disease and dysfunction (Park *et al.*, 2009). Exploration of the cellular and molecular mechanisms underlying air pollutant-induced pulmonary oxidative stress has focused on epithelial and immune cells, which directly interact with the full dose of inhaled materials. Lung fibroblasts reside immediately beneath the epithelial barrier throughout the airways, constitute approximately 75% of the total interstitial volume of the lung, and play a critical role in regulating respiratory tract structure, function, and disease (Bradley *et al.*, 1980; Kendall and Feghali-Bostwick, 2014; White, 2015); however, current testing approaches do not consider them as potential targets and/or mediators of the effects of inhaled chemical exposures.

Here, we demonstrate that exposure to the model oxidant diesel exhaust particulates causes transepithelial redox imbalance and oxidative stress in lung fibroblasts, despite their separation from the diesel exhaust particulates by a functional bronchial epithelial cell barrier. In addition, we observed that the transepithelial effects of diesel exhaust particulate exposure on the expression of oxidative stress-responsive genes in lung fibroblasts were similar or greater than in adjacent epithelial cells that received direct diesel exhaust particulate exposure (Figs. 4 and 5). Antioxidant pretreatment of fibroblasts partially mitigated the effects of direct diesel exhaust particulate exposure in adjacent epithelial cells, indicating that redox balance in lung fibroblasts plays a role in the response of neighboring bronchial epithelial cells (Figure 6). To the best of our knowledge, this is the first report describing the dynamics of the transepithelial effects of inhaled material exposure on intracellular hydrogen peroxide accumulation, global cellular glutathione oxidation, and oxidative stress-responsive gene expression and transcription factor activation in lung fibroblasts during an exposure time course. These findings are significant because they (1) indicate that exposure-induced redox imbalance and oxidative stress are not limited to epithelial and immune cells that come into direct contact with the toxicant; (2) demonstrate that lung fibroblasts are both a target of the transepithelial effects of diesel exhaust particulates exposure and a mediator of the response of adjacent bronchial epithelial cells to direct diesel exhaust particulate exposure; and (3) indicate that lung fibroblasts may be more sensitive to oxidative insult than adjacent bronchial epithelial cells.

Oxidative stress begins with the disruption of redox homeostasis via the generation of reactive oxygen species, such as hydrogen peroxide, and oxidation of the abundant antioxidant molecule glutathione (Rahman and MacNee, 1999). Increased cellular oxidative potential activates the transcription factor NRF2 via protein stabilization, leading to induction of oxidative stress-responsive genes (Cho *et al.*, 2006). Transepithelial diesel exhaust particulate exposure rapidly increased the accumulation of intracellular hydrogen peroxide and oxidation of glutathione to greater than 90% and 80% of values obtained by direct exposure to 1 mM hydrogen peroxide, respectively, in lung fibroblasts during the first 6 h of exposure (Figure 3). The timing of these events preceded peak activation of NRF2 that was greater in magnitude and duration in lung fibroblast than directly exposed bronchial epithelial cells (Figure 5); however, our ability to assess the kinetics of hydrogen peroxide accumulation and glutathione oxidation by live cell imaging was limited to 6 h due to apparent phototoxicity in lung fibroblasts during longer duration studies.

In vitro exposure of primary bronchial epithelial cells to diesel exhaust particulates induces the expression of oxidative stress-responsive targets such as HMOX1, NQO1, and PTGS2

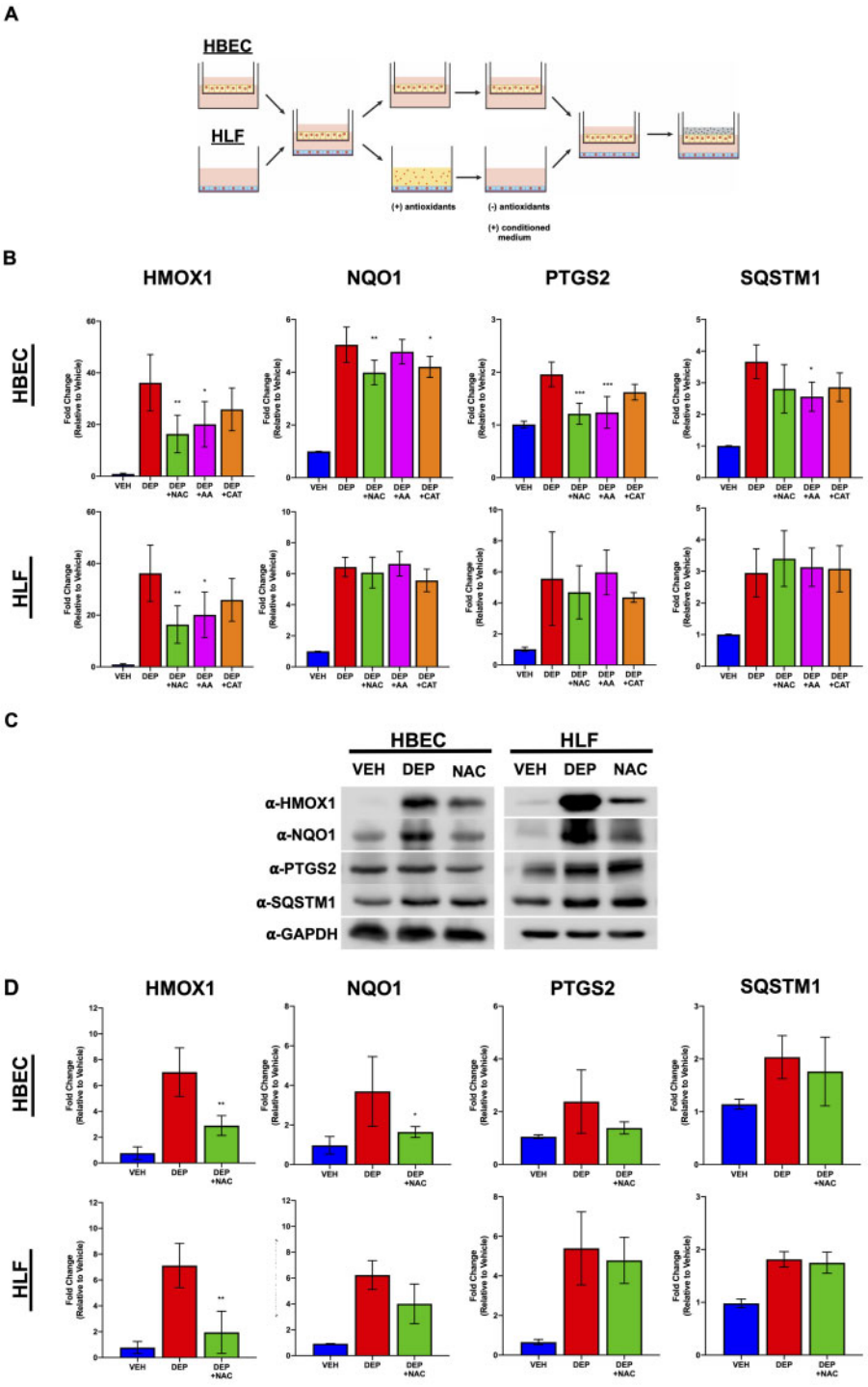

Figure 6. Effect of antioxidant pretreatment of lung fibroblasts (HLFs) on oxidative stress-responsive gene expression in both HLFs and bronchial epithelial cells (HBECs). A, Graphical depiction of antioxidant pretreatment protocol. HBECs and HLFs were seeded within wells or on Transwell inserts, respectively, and cocultured overnight. HBEC-containing inserts were removed and placed in conditioned medium whereas HLFs were treated with antioxidants N-acetyl-L-cysteine (NAC; 10 mM), L-ascorbic acid (AA; 10 mM), or catalase (CAT; 150 U/ml) for 1 h. The antioxidant-containing medium was then removed, conditioned medium was added, HBEC containing inserts were replaced, and cells were exposed to diesel exhaust particulates within the transepithelial exposure model. B, The induction of oxidative stress-responsive mRNA was assessed by qPCR for *HMOX1* ($n = 5$) and *PTGS2* ($n = 4$) following 6 h of exposure, and *NQO1* ($n = 5$) and *SQSTM1* ($n = 5$) following 24 h of exposure. C, HLFs were pretreated with N-acetylcysteine before transepithelial exposure for 8 or 24 h prior to the preparation of whole cell lysate and immunoblotting with the indicated antibodies. The immunoblots shown are representative of results obtained from 3 independent replicate exposures. D, Densitometry performed with FIJI for ImageJ and normalized to unexposed samples.

(Totlandsdal *et al.*, 2012; Zarcone *et al.*, 2016). Further, diesel exhaust particulate exposure upregulates SQSTM1, which plays a diverse role in cell physiology and regulates NRF2 activation (Katsuragi *et al.*, 2016), in the bronchial epithelial cell line BEAS-2B (Frias *et al.*, 2020). We observed the induction of all 4 genes at the transcriptional level in both bronchial epithelial cells and

lung fibroblasts/primary lung fibroblasts with similar kinetics despite the direct and transepithelial nature of their exposures, respectively. Given the presence of a functional epithelial barrier separating the lung fibroblasts from the diesel exhaust particulates (Figure 2), physical distance of the lung fibroblasts from the diesel exhaust particulates as a result of the coculture format (Figure 1B), and dilution of any factors released by exposed bronchial epithelial cells in culture medium, we interpreted these observations to indicate that lung fibroblasts are more responsive to oxidative insult than the neighboring bronchial epithelial cells. While our observations suggest that lung fibroblasts are more responsive to oxidative insult, our study was limited by the small number of target genes examined. In addition, we did not compare the effects of transepithelial and direct diesel exhaust particulate exposures in lung fibroblasts because direct exposure of lung fibroblasts to diesel exhaust particulates is not physiologically relevant in the healthy airway and the two formats represent independent biological scenarios with distinct dosimetry. Differences in susceptibility to oxidative insult between the two cell types may suggest that lung fibroblasts have relatively lower levels of cellular antioxidants such as reduced glutathione, thioredoxin, and NADPH-dependent oxidoreductases that play integral roles in cellular redox regulation (Rahman *et al.*, 2005); however, antioxidant pretreatment of lung fibroblasts had a minimal effect on mitigating their response to transepithelial diesel exhaust particulate exposure (Figure 6). Regardless of the mechanism, these observations demonstrate that the transepithelial effects of diesel exhaust particulate exposure cause oxidative stress in lung fibroblasts despite a lack of direct contact.

Exposure to inhaled chemicals, such as air pollutants, occupational chemicals, pharmaceuticals, and consumer products often occurs in a repeated/daily, or continuous, manner with a cumulative effect on the risk of adverse outcomes (United States Environmental Protection Agency, 2019, 2011). Differences among the effects of acute, subchronic, and chronic exposures/effects, as well as the underlying molecular mechanisms, are poorly understood. The persistent elevation of PTGS2, NQO1, and SQSTM1 in lung fibroblasts through 24 h of exposure (Figure 4) may have implications when extrapolating *in vitro* observations to these "real-world" multiexposure scenarios. PTGS2 catalyzes the generation of prostaglandins and thromboxanes from arachidonic acid and plays a role in of acute lung injury (Fukunaga *et al.*, 2005), development of pulmonary fibrosis (Lovgren *et al.*, 2006), and lung cancer outcomes (Wolff *et al.*, 1998). PTGS2 appears to play a dual role in the response to inhaled toxicants. PTGS2 metabolites are mediators of the bronchorestrictive- and obstructive-type effects of *in vivo* controlled human exposure to the air pollutant ozone in normal and asthmatic volunteers, respectively (Alexis *et al.*, 2000). Alternatively, PTGS2 deficiency increases oxidative stress markers in transgenic mice in a drug-induced model of pulmonary hypertension (Seta *et al.*, 2011) suggesting that PTGS2 is protective against pulmonary oxidative stress. The induction of PTGS2 in lung fibroblasts has also been suggested to be a contributing factor to the establishment of an inflammatory environment supportive of lung cancer and COPD development (Martey *et al.*, 2004). Lung fibroblasts isolated from COPD patients produce greater amounts of the PTGS2 product prostaglandin E2, which corresponded to reductions in the indicators of the fibroblast repair functions fibronectin-directed chemotaxis and collagen gel contraction. These repair functions were partially restored when COPD fibroblasts were treated with the PTGS2 inhibitor indomethacin (Togo *et al.*, 2008). The role of lung fibroblasts in regulating the local inflammatory environment, as well as tissue repair functions, suggests that the transepithelial diesel exhaust particulate-induced upregulation of PTGS2 that we observed may be a mechanism contributing to the ability of diesel exhaust exposure to cause lung cancer (Attfield *et al.*, 2012; Silverman *et al.*, 2012) and COPD (Hart *et al.*, 2012). Further, our lack of observation of PTGS2 protein induction in bronchial epithelial cells (Figs. 4C and 4D) suggests that fibroblasts are playing a greater role in the diesel exhaust particulate-induced development of these diseases than has been previously considered.

NQO1 catalyzes the first step in quinone metabolism via two-electron reduction to their hydroquinone form (Chen *et al.*, 2000; Ross and Siegel, 2017). Quinones are present in diesel exhaust particulates as well as a diverse range of consumer products and environmental pollutants, and quinone metabolism is involved in the activation of some prodrugs. Prolonged elevation of NQO1 protein may increase the ability of cells to detoxify quinones by two-electron reduction to hydroquinones in subsequent exposures; however, this may also predispose cells for greater damage if the hydroquinone metabolite of the secondary exposure material is redox active or capable of rearrangement to form a reactive alkylating species (Kennedy *et al.*, 1980; Ross and Siegel, 2017). SQSTM1 plays a diverse role in the regulation of cellular homeostasis (Katsuragi *et al.*, 2016). The cytoprotective effects of SQSTM1 involve its functions both in the activation of NRF2 and as an autophagy adapter protein, which intersect through the SQSTM1 targeted degradation of KEAP1, a negative regulator of NRF2 activation (Copple *et al.*, 2010; Divya *et al.*, 2017; Katsuragi *et al.*, 2016). In this study, activation of NRF2 in both bronchial epithelial cells and lung fibroblasts preceded changes in SQSTM1 protein levels during the acute exposure time course (Figs. 4 and 5); however, increased SQSTM1 in both cell types at 24 h may serve a cytoprotective role by potentiating the activation of NRF2 in response to a secondary exposure event. Alternatively, elevated SQSTM1 levels can indicate a deficiency in autophagy, which is a contributing factor to bleomycin-induced pulmonary fibrosis (Divya *et al.*, 2017) and the inhibition of autophagy alone is sufficient to drive lung fibroblast to myofibroblast differentiation, a key feature of idiopathic pulmonary fibrosis (Araya *et al.*, 2013). Further, SQSTM1 protein is enriched in fibroblastic foci in lungs of idiopathic pulmonary fibrosis patients (Hill *et al.*, 2019). Diesel exhaust particulate exposure was recently reported to cause lung fibrosis in a mouse model (Kim *et al.*, 2016); however, currently there is not an established link between diesel exhaust particulate exposure and pulmonary fibrosis in humans. In the absence of overt lung fibrosis in humans, persistent accumulation of SQSTM1 in response to multiple exposures may deregulate autophagy and contribute to the development of other subchronic/chronic pulmonary diseases (Mizumura *et al.*, 2012). Additional studies are required to determine whether the persistence of these induced proteins through 24 h of exposure alters the responses of lung fibroblasts and adjacent epithelial cells in a comparison of single and multiple exposure scenarios. Future studies are also required to further explore the transepithelial effects of exposures to diesel exhaust particulates and other inhaled chemicals on lung fibroblasts, and their role in inhalation toxicology.

Improving the physiologic relevance of *in vitro* airway models by incorporating *in vivo* biological complexity is critical to accurate and representative *in vitro* inhaled chemical research and testing. Here, we used an indirect coculture model designed to examine the direct and transepithelial effects of inhaled chemical exposures on bronchial epithelial cells and lung fibroblasts,

respectively, in a parallel and cell type-specific manner. The model utilizes commercially available components to ensure accessibility and is scalable to accommodate a broad range of assay sample size and throughput requirements. Further, this model is relatively low cost with the Transwell insert itself constituting the majority of the cost per assay. These characteristics allow for the acquisition of dose and time course data across multiple endpoints, providing a more complete assessment of exposure effects, and promote the development of computational models to further increase the efficiency and accuracy of chemical testing. Although the indirect nature of the model allows for the separation of the epithelial and fibroblast compartments for parallel and cell type-specific analysis, the physical separation of the bronchial epithelial cells and fibroblasts limits the ability of our indirect model to represent the role of direct cell-cell interactions in exposure outcomes. Cell-cell interactions can be represented in analogous multicellular direct coculture models; however, application of these models in cell type-specific analysis using many common assays (eg, transcriptional analysis, Western blotting, epigenetics) is limited by the impracticality of disarticulating the interacting cell types once the model is assembled. Ultimately, both direct and indirect coculture models are needed to provide a comprehensive and accurate approach to inhaled chemical research and testing. Future studies of direct and transepithelial exposure effects will also benefit from the incorporation of additional cell types that are present *in vivo* (eg, immune cells) to further improve physiological relevance.

In conclusion, our findings demonstrate that diesel exhaust particulates cause transepithelial disruption of redox homeostasis and induces oxidative stress in lung fibroblasts. These observations indicate that current *in vitro* bronchial epithelial monoculture models alone do not fully represent the adverse effects of toxicant exposures on the airways. In addition, we found that lung fibroblasts may, in fact, be more responsive to oxidative insult than the directly exposed bronchial epithelial cells that have been previously studied. This illustrates the value of using coculture *in vitro* models to define the cellular and molecular effects and mechanisms involved in toxicant exposures to improve the scope and physiological relevance in toxicity research and testing.

SUPPLEMENTARY DATA

Supplementary data are available at *Toxicological Sciences* online.

AUTHOR CONTRIBUTIONS

The transepithelial exposure model was designed by S.D.M. and originally developed by S.D.M. and N.A.M. S.D.M. and S.C.F. designed the study. S.C.F, N.A.M., P.A., and E.R.A. conducted the study. S.C.F. and S.D.M. wrote the manuscript.

ACKNOWLEDGMENTS

The authors would like to thank Dr Kymberly Gowdy for critical review of the manuscript. They would also like to thank Dr Jay Snouwaert for assistance provided in the construction of the pLV-dfROX vector, and Dr Scott Randell for kindly providing primary normal lung fibroblasts. Dr Andy Ghio collected primary bronchial epithelial cells and Lisa A. Dailey established, maintained, and differentiated primary bronchial epithelial cultures.

FUNDING

National Institutes of Health (Grant/Award No.: P30 CA016086); U.S. Environmental Protection Agency intramural funding (S.D.M.); UNC/EPA Toxicology Training Agreement (CR-83591401 supporting S.C.F.); the Colgate-Palmolive Postdoctoral Fellowship (S.C.F.). This research was supported by U.S. Environmental Protection Agency (Agreement No. CR83578501) to Dr David Peden (UNC Center for Environmental Medicine, Asthma, and Lung Biology). The Microscopy Services Laboratory, Department of Pathology and Laboratory Medicine, is supported in part by P30 CA016086 Cancer Center Core Support Grant to the UNC Lineberger Comprehensive Cancer Center.

DECLARATION OF CONFLICTING INTERESTS

The authors declared no potential conflicts of interest with respect to the research, authorship, and/or publication of this article.

REFERENCES

Alexis, N., Urch, B., Tarlo, S., Corey, P., Pengelly, D., O'Byrne, P., and Silverman, F. (2000). Cyclooxygenase metabolites play a different role in ozone-induced pulmonary function decline in asthmatics compared to normals. *Inhal. Toxicol.* **12**, 1205–1224.

Anderson, J. O., Thundiyil, J. G., and Stolbach, A. (2012). Clearing the air: A review of the effects of particulate matter air pollution on human health. *J. Med. Toxicol.* **8**, 166–175.

Araya, J., Kojima, J., Takasaka, N., Ito, S., Fujii, S., Hara, H., Yanagisawa, H., Kobayashi, K., Tsurushige, C., Kawaishi, M., *et al.* (2013). Insufficient autophagy in idiopathic pulmonary fibrosis. *Am. J. Physiol. Lung Cell. Mol. Physiol.* **304**, 56–69.

Attfield, M. D., Schleiff, P. L., Lubin, J. H., Blair, A., Stewart, P. A., Vermeulen, R., Coble, J. B., and Silverman, D. T. (2012). The diesel exhaust in miners study: A cohort mortality study with emphasis on lung cancer. *J. Natl. Cancer Inst.* **104**, 869–883.

Balásházy, I., Hofmann, W., and Heistracher, T. (2003). Local particle deposition patterns may play a key role in the development of lung cancer. *J. Appl. Physiol.* **94**, 1719–1725.

Baulig, A., Garlatti, M., Bonvallot, V., Marchand, A., Barouki, R., Marano, F., and Baeza-Squiban, A. (2003). Involvement of reactive oxygen species in the metabolic pathways triggered by diesel exhaust particles in human airway epithelial cells. *Am. J. Physiol. Lung Cell. Mol. Physiol.* **285**, L671–679.

Bayram, H., Devalia, J. L., Sapsford, R. J., Ohtoshi, T., Miyabara, Y., Sagai, M., and Davies, R. J. (1998). The effect of diesel exhaust particles on cell function and release of inflammatory mediators from human bronchial epithelial cells *in vitro*. *Am. J. Respir. Cell Mol. Biol.* **18**, 441–448.

Bradley, K. H., Kawanami, O., Ferrans, V. J., and Crystal, R. G. (1980). The fibroblast of human lung alveolar structures: A differentiated cell with a major role in lung structure and function. *Methods Cell Biol.* **21**, 37–64.

Carlsten, C., MacNutt, M. J., Zhang, Z., Sava, F., and Pui, M. M. (2014). Anti-oxidant N-acetylcysteine diminishes diesel

exhaust-induced increased airway responsiveness in person with airway hyper-reactivity. *Toxicol. Sci.* **139**, 479–487.

Chen, S., Wu, K., and Knox, R. (2000). Structure-function studies of DT-diaphorase (NQO1) and NRH: Quinone oxidoreductase (NQO2). *Free Radic. Biol. Med.* **29**, 276–284.

Cheng, W.-Y., Currier, J., Bromberg, P. A., Silbajoris, R., Simmons, S. O., and Samet, J. M. (2012). Linking oxidative events to inflammatory and adaptive gene expression induced by exposure to an organic particulate matter component. *Environ. Health Perspect.* **120**, 267–274.

Cho, H.-Y., Reddy, S. P., and Kleeberger, S. R. (2006). Nrf2 defends the lung from oxidative stress. *Antioxid. Redox Signal.* **8**, 76–87.

Churg, A., and Vedal, S. (1996). Carinal and tubular airway particle concentrations in the large airways of non-smokers in the general population: Evidence for high particle concentration at airway carinas. *Occup. Environ. Med.* **53**, 553–558.

Collins, F. S., Gray, G. M., and Bucher, J. R. (2008). Transforming environmental health protection. *Science*, **319**, 906–907.

Copple, I. M., Lister, A., Obeng, A. D., Kitteringham, N. R., Jenkins, R. E., Layfield, R., Foster, B. J., Goldring, C. E., and Park, B. K. (2010). Physical and functional interaction of sequestosome 1 with Keap1 regulates the Keap1-Nrf2 cell defense pathway. *J. Biol. Chem.* **285**, 16782–16788.

Cozens, A. L., Yezzi, M. J., Kunzelmann, K., Ohrui, T., Chin, L., Eng, K., Finkbeiner, W. E., Widdicombe, J. H., and Gruenert, D. C. (1994). CFTR expression and chloride secretion in polarized immortal human bronchial epithelial cells. *Am. J. Respir. Cell Mol. Biol.* **10**, 38–47.

Danielsen, P. H., Loft, S., and Møller, P. (2008). DNA damage and cytotoxicity in type II lung epithelial (A549) cell cultures after exposure to diesel exhaust and urban street particles. *Part. Fibre Toxicol.* **5**, 1–12.

Deavall, D. G., Martin, E. A., Horner, J. M., and Roberts, R. (2012). Drug-induced oxidative stress and toxicity. *J. Toxicol.* **2012**, 1–13.

Divya, T., Sureshkumar, A., and Sudhandiran, G. (2017). Autophagy induction by celastrol augments protection against bleomycin-induced experimental pulmonary fibrosis in rats: Role of adaptor protein p62/SQSTM1. *Pulm. Pharmacol. Ther.* **45**, 47–61.

Ermakova, Y. G., Bilan, D. S., Matlashov, M. E., Mishina, N. M., Markvicheva, K. N., Subach, O. M., Subach, F. V., Bogeski, I., Hoth, M., Enikolopov, G., *et al.* (2014). Red fluorescent genetically encoded indicator for intracellular hydrogen peroxide. *Nat. Commun.* **5**, 5222.

Faber, S., Mallek, N., and McCullough, S. (2019). Measurement of trans-epithelial electrical resistance with EVOM2 and chopstick electrode. *Protoc. Exch.* DOI: 10.21203/rs.2.20356/v1.

Faber, S., and McCullough, S. (2019). FITC-dextran trans-epithelial permeability assay. *Protoc. Exch.* DOI: 10.21203/rs.2.20495/v1.

Faber, S., Vitucci, E., and McCullough, S. (2020). Transduction of cultured cells with recombinant lentiviral particles. *Protoc. Exch.* DOI: 10.21203/rs.2.20633/v1.

Feng, W., Guo, J., Huang, H., Xia, B., Liu, H., Li, J., Lin, S., Li, T., Liu, J., and Li, H. (2015). Human normal bronchial epithelial cells: A novel *in vitro* cell model for toxicity evaluation. *PLoS One* **10**, e0123520.

Frias, D. P., Gomes, R. L. N., Yoshizaki, K., Carvalho-Oliveira, R., Matsuda, M., Junqueira, M. de S., Teodoro, W. R., Vasconcellos, P. de C., Pereira, D. C. de A., da Conceição, P. R., *et al.* (2020). Nrf2 positively regulates autophagy antioxidant response in human bronchial epithelial cells exposed to diesel exhaust particles. *Sci. Rep.* **10**, 1–13.

Fukunaga, K., Kohli, P., Bonnans, C., Fredenburgh, L. E., and Levy, B. D. (2005). Cyclooxygenase 2 plays a pivotal role in the resolution of acute lung injury. *J. Immunol.* **174**, 5033–5039.

Gibbs-Flournoy, E. A., Simmons, S. O., Bromberg, P. A., Dick, T. P., and Samet, J. M. (2013). Monitoring intracellular redox changes in ozone-exposed airway epithelial cells. *Environ. Health Perspect.* **121**, 312–317.

Gonzalez-Mariscal, L., Quiros, M., and Diaz-Coranguez, M. (2011). ZO proteins and redox-dependent processes. *Antioxid. Redox Signal.* **15**, 1235–1253.

Han, J. Y., Takeshita, K., and Utsumi, H. (2001). Noninvasive detection of hydroxyl radical generation in lung by diesel exhaust particles. *Free Radic. Biol. Med.* **30**, 516–525.

Hanson, G. T., Aggeler, R., Oglesbee, D., Cannon, M., Capaldi, R. A., Tsien, R. Y., and Remington, S. J. (2004). Investigating mitochondrial redox potential with redox-sensitive green fluorescent protein indicators. *J. Biol. Chem.* **279**, 13044–13053.

Hart, J. E., Eisen, E. A., and Laden, F. (2012). Occupational diesel exhaust exposure as a risk factor for chronic obstructive pulmonary disease. *Curr. Opin. Pulm. Med.* **18**, 151–154.

Hill, C., Li, J., Liu, D., Conforti, F., Brereton, C. J., Yao, L., Zhou, Y., Alzetani, A., Chee, S. J., Marshall, B. G., *et al.* (2019). Autophagy inhibition-mediated epithelial-mesenchymal transition augments local myofibroblast differentiation in pulmonary fibrosis. *Cell Death Dis.* **10**, 591.

Itoh, M., and Bissell, M. J. (2003). The organization of tight junctions in epithelia: Implications for mammary gland biology and breast tumorigenesis. *J. Mammary Gland Biol. Neoplasia* **8**, 449–462.

Ji, J., Upadhyay, S., Xiong, X., Malmlof, M., Sandstrom, T., Gerde, P., and Palmberg, L. (2018). Multi-cellular human bronchial models exposed to diesel exhaust particles: Assessment of inflammation, oxidative stress and macrophage polarization. *Part. Fibre Toxicol.* **15**, 19.

Katsuragi, Y., Ichimura, Y., and Komatsu, M. (2016). Regulation of the Keap1-Nrf2 pathway by p62/SQSTM1. *Curr. Opin. Toxicol.* **1**, 54–61.

Kemmerer, Z. A., Ader, N. R., Mulroy, S. S., and Eggler, A. L. (2015). Comparison of human Nrf2 antibodies: A tale of two proteins. *Toxicol. Lett.* **238**, 83–89.

Kendall, R. T., and Feghali-Bostwick, C. A. (2014). Fibroblasts in fibrosis: Novel roles and mediators. *Front. Pharmacol.* **5**, 123.

Kennedy, K. A., Sartorelli, A. C., and Rockwell, S. (1980). Preferential activation of mitomycin C to cytotoxic metabolites by hypoxic tumor cells. *Cancer Res.* **40**, 2356–2360.

Kim, B. G., Lee, P. H., Lee, S. H., Kim, Y. E., Shin, M. Y., Kang, Y., Bae, S. H., Kim, M. J., Rhim, T. Y., Park, C. S., *et al.* (2016). Long-term effects of diesel exhaust particles on airway inflammation and remodeling in a mouse model. *Allergy Asthma Immunol. Res.* **8**, 246–256.

Kleinstreuer, N. C., Yang, J., Berg, E. L., Knudsen, T. B., Richard, A. M., Martin, M. T., Reif, D. M., Judson, R. S., Polokoff, M., Dix, D. J., *et al.* (2014). Phenotypic screening of the ToxCast chemical library to classify toxic and therapeutic mechanisms. *Nat. Biotechnol.* **32**, 583–591.

Lau, A., Tian, W., Whitman, S. A., and Zhang, D. D. (2013). The predicted molecular weight of Nrf2: It is what it is not. *Antioxid. Redox Signal.* **18**, 91–93.

Lehmann, A. D., Blank, F., Baum, O., Gehr, P., and Rothen-Rutishauser, B. M. (2009). Diesel exhaust particles modulate the tight junction protein occludin in lung cells *in vitro*. *Part. Fibre Toxicol.* **6**, 26.

Li, N., Xia, T., and Nel, A. E. (2008). The role of oxidative stress in ambient particulate matter-induced lung diseases and its

implications in the toxicity of engineered nanoparticles. *Free Radic. Biol. Med.* **44**, 1689–1699.

Lodovici, M., and Bigagli, E. (2011). Oxidative stress and air pollution exposure. *J. Toxicol.* **2011**, 1–9.

Lovgren, A. K., Jania, L. A., Hartney, J. M., Parsons, K. K., Audoly, L. P., FitzGerald, G. A., Tilley, S. L., and Koller, B. H. (2006). COX-2-derived prostacyclin protects against bleomycin-induced pulmonary fibrosis. *Am. J. Physiol. Lung Cell. Mol. Physiol.* **291**, 144–156.

MacNee, W. (2001). Oxidative stress and lung inflammation in airways disease. *Eur. J. Pharmacol.* **429**, 195–207.

Martey, C. A., Pollock, S. J., Turner, C. K., O'Reilly, K. M. A., Baglole, C. J., Phipps, R. P., and Sime, P. J. (2004). Cigarette smoke induces cyclooxygenase-2 and microsomal prostaglandin E2 synthase in human lung fibroblasts: Implications for lung inflammation and cancer. *Am. J. Physiol. Lung Cell. Mol. Physiol.* **287**, 981–991.

Martonen, T. B. (1992). Deposition patterns of cigarette smoke in human airways. *Am. Ind. Hyg. Assoc. J.* **53**, 6–18.

Martonen, T. B., Yang, Y., and Xue, Z. Q. (1994). Effects of carinal ridge shapes on lung airstreams. *Aerosol Sci. Technol.* **21**, 119–136.

Mazzarella, G., Ferraraccio, F., Prati, M. V., Annunziata, S., Bianco, A., Mezzogiorno, A., Liguori, G., Angelillo, I. F., and Cazzola, M. (2007). Effects of diesel exhaust particles on human lung epithelial cells: An *in vitro* study. *Respir. Med.* **101**, 1155–1162.

McCullough, S. D. (2019). Production and concentration of recombinant lentiviral particles. *Protoc. Exch.* DOI: 10.21203/rs.2.20494/v1.

McCullough, S. D., Xu, X., Dent, S. Y. R., Bekiranov, S., Roeder, R. G., and Grant, P. A. (2012). Reelin is a target of polyglutamine expanded ataxin-7 in human spinocerebellar ataxia type 7 (SCA7) astrocytes. *Proc. Natl. Acad. Sci. U.S.A.* **109**, 21319–21324.

McNabb, N., Mallek, N., Faber, S., and McCullough, S. (2019). Trans-epithelial exposure model (TEEM)—Epithelial cells and fibroblasts. *Protoc. Exch.* DOI: 10.21203/rs.2.18675/v1.

McNabb, N., and McCullough, S. (2019a). Collagen coating for tissue culture. *Protoc. Exch.* DOI: 10.21203/rs.2.20355/v2.

McNabb, N., and McCullough, S. (2019b). Culture of 16HBE14o− cells. *Protoc. Exch.* DOI: 10.21203/rs.2.20353/v1.

McNabb, N., and McCullough, S. (2019c). Culture of IMR90 cells. *Protoc. Exch.* DOI: 10.21203/rs.2.20354/v1.

McNabb, N., and McCullough, S. (2020). Isolation of total RNA with the life technologies PureLink kit. *Protoc. Exch.* DOI: 10.21203/rs.2.21222/v1.

Mizumura, K., Cloonan, S. M., Haspel, J. A., and Choi, A. M. K. (2012). The emerging importance of autophagy in pulmonary diseases. *Chest* **142**, 1289–1299.

National Research Council. (2007). *Toxicity Testing in the 21st Century: A Vision and Strategy*. The National Academies Press, Washington, DC.

Nguyen, T., Nioi, P., and Pickett, C. B. (2009). The Nrf2-antioxidant response element signaling pathway and its activation by oxidative stress. *J. Biol. Chem.* **284**, 13291–13295.

Nichols, W., Murphy, D., Cristofalo, V., Toji, L., Greene, A., and Dwight, A. (1977). Characterization of a new human diploid cell strain, IMR-90. *Science*, **196**, 60–63.

Okubo, T., Hosaka, M., and Nakae, D. (2015). *In vitro* effects induced by diesel exhaust at an air-liquid interface in a human lung alveolar carcinoma cell line A549. *Exp. Toxicol. Pathol.* **67**, 383–388.

Park, H. S., Kim, S. R., and Lee, Y. C. (2009). Impact of oxidative stress on lung diseases. *Respirology* **14**, 27–38.

Pfaffl, M. W. (2001). A new mathematical model for relative quantification in real-time RT-PCR. *Nucleic Acids Res.* **29**, e45.

Poli, G., Leonarduzzi, G., Biasi, F., and Chiarpotto, E. (2004). Oxidative stress and cell signalling. *Curr. Med. Chem.* **11**, 1163–1182.

Rahman, I., Biswas, S. K., Jimenez, L. A., Torres, M., and Forman, H. J. (2005). Glutathione, stress responses, and redox signaling in lung inflammation. *Antioxid. Redox Signal.* **7**, 42–59.

Rahman, I., and MacNee, W. (1999). Lung glutathione and oxidative stress: Implications in cigarette smoke-induced airway disease. *Am. J. Physiol.* **277**, 1067–1088.

Rao, X., Zhong, J., Brook, R. D., and Rajagopalan, S. (2018). Effect of particulate matter air pollution on cardiovascular oxidative stress pathways. *Antioxid. Redox Signal.* **28**, 797–818.

Rodrigues da Silva, M., Schapochnik, A., Peres Leal, M., Esteves, J., Bichels Hebeda, C., Sandri, S., Pavani, C., Ratto Tempestini Horliana, A. C., Farsky, S. H. P., and Lino-Dos-Santos-Franco, A. (2018). Beneficial effects of ascorbic acid to treat lung fibrosis induced by paraquat. *PLoS One* **13**, e0205535.

Ross, D., and Siegel, D. (2017). Functions of NQO1 in cellular protection and CoQ10 metabolism and its potential role as a redox sensitive molecular switch. *Front. Physiol.* **8**, 1–10.

Rynning, I., Neca, J., Vrbova, K., Libalova, H., Rossner, P., Holme, J. A., Gützkow, K. B., Afanou, A. K. J., Arnoldussen, Y. J., Hruba, E., *et al.* (2018). *In Vitro* transformation of human bronchial epithelial cells by diesel exhaust particles: gene expression profiling and early toxic responses. *Toxicol. Sci.* **166**, 51–64.

Saatian, B., Rezaee, F., Desando, S., Emo, J., Chapman, T., Knowlden, S., and Georas, S. N. (2013). Interleukin-4 and interleukin-13 cause barrier dysfunction in human airway epithelial cells. *Tissue Barriers* **1**, e24333.

Sagai, M., Saito, H., Ichinose, T., Kodama, M., and Mori, Y. (1993). Biological effects of diesel exhaust particles. I. *In vitro* production of superoxide and *in vivo* toxicity in mouse. *Free Radic. Biol. Med.* **14**, 37–47.

Schindelin, J., Arganda-Carreras, I., Frise, E., Kaynig, V., Longair, M., Pietzsch, T., Preibisch, S., Rueden, C., Saalfeld, S., Schmid, B., *et al.* (2012). Fiji: An open-source platform for biological-image analysis. *Nat. Methods* **9**, 676–682.

Schlesinger, R. B., and Lippmann, M. (1972). Particle deposition in casts of the human upper tracheobronchial tree. *Am. Ind. Hyg. Assoc. J.* **33**, 237–251.

Schlesinger, R. B., and Lippmann, M. (1978). Selective particle deposition and bronchogenic carcinoma. *Environ. Res.* **15**, 424–431.

Seta, F., Rahmani, M., Turner, P. V., and Funk, C. D. (2011). Pulmonary oxidative stress is increased in cyclooxygenase-2 knockdown mice with mild pulmonary hypertension induced by monocrotaline. *PLoS One* **6**, e23439.

Silverman, D. T., Samanic, C. M., Lubin, J. H., Blair, A. E., Stewart, P. A., Vermeulen, R., Coble, J. B., Rothman, N., Schleiff, P. L., Travis, W. D., *et al.* (2012). The diesel exhaust in miners study: A nested case-control study of lung cancer and diesel exhaust. *J. Natl. Cancer Inst.* **104**, 855–868.

Singh, P., DeMarini, D. M., Dick, C. A. J., Tabor, D. G., Ryan, J. V., Linak, W. P., Kobayashi, T., and Gilmour, M. I. (2004). Sample characterization of automobile and forklift diesel exhaust particles and comparative pulmonary toxicity in mice. *Environ. Health Perspect.* **112**, 820–825.

Srinivasan, B., Kolli, A. R., Esch, M. B., Abaci, H. E., Shuler, M. L., and Hickman, J. J. (2015). TEER measurement techniques for *in vitro* barrier model systems. *J. Lab. Autom.* **20**, 107–126.

Steiner, S., Bisig, C., Petri-Fink, A., and Rothen-Rutishauser, B. (2016). Diesel exhaust: Current knowledge of adverse effects and underlying cellular mechanisms. *Arch. Toxicol.* **90**, 1541–1553.

Togo, S., Holz, O., Liu, X., Sugiura, H., Kamio, K., Wang, X., Kawasaki, S., Ahn, Y., Fredriksson, K., Skold, C. M., *et al.* (2008). Lung fibroblast repair functions in patients with chronic obstructive pulmonary disease are altered by multiple mechanisms. *Am. J. Respir. Crit. Care Med.* **178**, 248–260.

Totlandsdal, A. I., Herseth, J. I., Bølling, A. K., Kubátová, A., Braun, A., Cochran, R. E., Refsnes, M., Øvrevik, J., and Låg, M. (2012). Differential effects of the particle core and organic extract of diesel exhaust particles. *Toxicol. Lett.* **208**, 262–268.

United States Environmental Protection Agency. (2011). *Air Quality Criteria and Related Photochemical Oxidants*. EPA/600/R-10/07A. US Environmental Protection Agency, Research Triangle Park, NC.

United States Environmental Protection Agency. (2019). *Integrated Science Assessment (ISA) for Particulate Matter*. EPA/600/R-19/188. US Environmental Protection Agency, Research Triangle Park, NC.

Valavanidis, A., Vlachogianni, T., Fiotakis, K., and Loridas, S. (2013). Pulmonary oxidative stress, inflammation and cancer: Respirable particulate matter, fibrous dusts and ozone as major causes of lung carcinogenesis through reactive oxygen species mechanisms. *Int. J. Environ. Res. Public Health* **10**, 3886–3907.

Wages, P. A., Silbajoris, R., Speen, A., Brighton, L., Henriquez, A., Tong, H., Bromberg, P. A., Simmons, S. O., and Samet, J. M. (2014). Role of H_2O_2 in the oxidative effects of zinc exposure in human airway epithelial cells. *Redox Biol.* **3**, 47–55.

White, E. S. (2015). Lung extracellular matrix and fibroblast function. *Ann. Am. Thorac. Soc.* **12**, S30–33.

Wolff, H., Saukkonen, K., Anttila, S., Karjalainen, A., Vainio, H., and Ristimäki, A. (1998). Expression of cyclooxygenase-2 in human lung carcinoma. *Cancer Res.* **58**, 4997–5001.

Zarcone, M. C., Duistermaat, E., van Schadewijk, A., Jedynska, A., Hiemstra, P. S., and Kooter, I. M. (2016). Cellular response of mucociliary differentiated primary bronchial epithelial cells to diesel exhaust. *Am. J. Physiol. Lung Cell. Mol. Physiol.* **311**, L111–123.

Zhang, Z., Kleinstreuer, C., Donohue, J. F., and Kim, C. S. (2005). Comparison of micro- and nano-size particle depositions in a human upper airway model. *J. Aerosol Sci.* **36**, 211–233.